(Received 23 May 2025, Accepted 17 August 2025, Scheduled 31 August 2025)

Enhancement and Optimization of High-Power Ku-Band Metallic Waveguide Radar Array Antenna: Large Efficiency, Wide Band and Low Side Lobe Level

Ibrahim S. Mohamed[1,*] and Mahmoud Abdalla[2]

[1] *Electronic Engineering Department, Military Technical College, Cairo, Egypt*
[2] *Electronic Engineering Department, Military Technical Research Center, Cairo, Egypt*

ABSTRACT: In this paper, the design of a cavity-backed slot antenna array with wideband operation and low sidelobe levels is introduced. A high gain metallic antenna array is designed using rectangular waveguides in both the feeding network and cavity-back slots, where a 16×16 array antenna is built with 8×8 subarrays. The antenna is fabricated using direct laser sintering (DLS) and computer numerical control (CNC) milling technology on both sides of each layer to guarantee no field leakage between antenna layers. For the sake of achieving a wide bandwidth in such array, a 1-to-64-way corporate feeding network is used to distribute the power in the lower feeding layer to excite the coupling apertures beneath the subarrays. The excited power coefficients through the array aperture are tapered using quasi-Taylor synthesis, with an even phase so the modified uneven power waveguide-splitter is designed to taper the field amplitudes within the feeding network till reaching the radiating slots. The array achieved a 14% bandwidth, a gain of more than 31.25 dBi over 1.85 GHz, sidelobe levels higher than 23 dB, and cross-polarization levels better than -40 dB, according to measured data.

1. INTRODUCTION

High gain radar antennas are preferred to be designed as metallic antennas instead of printed planar antennas especially at high frequencies, despite the light weight of planar antennas since these kinds of antennas suffer from high ohmic losses [1–3], lossy feeding network [4–7]. The antennas with high gain and low sidelobe levels are involved in many applications nowadays [8, 9]. Metallic antennas using waveguide technology are perfect for high power handling capability, high radiation efficiency, enormous realization, low losses, small size, high mechanical robustness, and high radiation efficiency [10]. Also, for high-speed point-to-point fixed wireless access systems, a high-gain and wideband array antenna is necessary [11]. A waveguide slot array antenna's feeding circuits can be basically divided into two types: series-feed and parallel-feed. Some of the metallic antennas have the drawback of narrow operating bandwidth due to using a series feed network in the feeding layer. Long-line effect often causes the bandwidth of a series-fed array antenna to shrink as the array size increases [12, 13]. In parallel-feeding networks, due to their complex three-dimensional feeding structure, waveguide slot array antennas with parallel feeds are typically large and are not appropriate for production in large quantities [14–16]. The design limitations of the feed waveguide in parallel feed are improved for a broader bandwidth using a multiple layer architecture. For this type of antenna, a corporate-fed array would be appropriate, and the feed waveguide's design limitation for greater bandwidth is improved by utilizing a multiple layer construction since cavity backed slot antennas have the advantage of wide bandwidth.

The proposed antenna in this work is fabricated using a combination of direct metal laser sintering (DLS) and computer numerical control (CNC) milling technologies. Also, there is an important point in this design that it is milled on both sides to decrease any electromagnetic (EM) leakage between multilayers of the slotted cavity backed antenna, where all layers are fixed together using only screws without any sealing filler materials. Other different slotted cavity backed array antennas at higher frequencies especially for millimeter-wave antennas are fabricated using diffusion bonding technology [17–21], through etching the required designs in the copper sheets and bonding these sheets together under high pressure and temperature (about 1000) in a vacuum, in order to reach the maximum limit in the precision of fabrication for very small dimensions in the array design that CNC technology cannot reach, but there is no need for such technology in the Ku-band antennas, and it is preferred to use the advantage of CNC milling precision in the fabrication that is low in cost. Some other work has been done such as the arrays using 3D printing technology [22–24].

To achieve a broad bandwidth and good radiation efficiency in the 12-GHz band, a double-layer slot array antenna consisting of a parallel feed waveguide and many 2×4-element cavity-backed subarrays is proposed in [25, 26]. To excite each element in phase, the two elements on the center-fed subarray are separated by nearly a guided wavelength in the E-plane direction. High side-lobe values of 8.8 dB were consequently seen in the E-plane pattern. The cavity backed slot antenna

* Corresponding author: Ibrahim Samy Mohamed (ibrahim.s.mahmoud@ieee.org).

has a 33.7 dB gain, 85% efficiency, and 12% bandwidth for VSWR < 2. A two-layer slotted waveguide antenna array with 24×24 elements in [27] achieves a gain of 33.8 dB at both frequencies 41.5 and 42.5 GHz, but suffers from low efficiency and narrow bandwidth of 51% and 5.5%, respectively.

The basic architecture for radiating design is proposed in the 60 GHz band in [17], where a hollow waveguide slot array antenna of 16×16 radiating elements with a corporate feed and uniform amplitude tapering along the array exhibits excellent gain (32-dB) and good efficiency (80%) over a wide bandwidth in the millimeter-wave region. In the multilayer corporate-feed waveguide slot array, the radiating element spacing is constant within less than a free-space wavelength. In [18] and [19], a 45° linearly polarized slot array antenna with an extra radiating layer reduces the sidelobe level (SLL) in both E- (25.5 dB) and H-planes (26.1 dB) in the 60 GHz band and in both E- and W-band. The antenna in [18] is designed using a parallel corporate feeding network to get a high efficiency of 70% and 32-dB gain over 5 GHz. The antenna in [19] consists of 8×8 subarrays of 16×16 radiating elements designed to have a broad bandwidth of 25.7% for VSWR < 1.5, antenna efficiency of 86.6%, low sidelobe level of 27.1 dB, first sidelobe level (FSLL) measured at a center frequency of 78.5 GHz, gain of 31.4 dB, and low cross polarization discrimination (XPD) of 30 dB over the bandwidth.

In this paper, a high power multilayer 16×16 waveguide slot array antenna is designed and optimized for sidelobe suppression with the aid of a double layer feeding network that has been implemented using an 8×8 corporate-feed network of 1–64 way power-splitting waveguide in a layer to excite an upper layer of 8×8 cavity array through apertures at the ends the waveguides. This solves the problem of insufficient space availability to design an efficient 16×16 slotted array with only one corporate feeding layer. The aperture power distribution is based on Taylor distribution, and the array factor (AF) is synthesized as an example. Only a quarter of the feed circuit due to the symmetry is designed by assembling H-plane T-junctions with uneven power splitting to realize the desirable aperture distribution.

The paper is organized as follows. The reason for choosing the high-power metallic waveguide arrays and the performance of other previous works are handled in Section 1. Section 2 is mainly divided into 2 parts: 1. 2×2 even power distribution subarray building cell, 2. the array synthesis through amplitude tapering techniques to reduce the sidelobe level, with the feeding network designed with the optimized balanced-phase uneven-power splitters used to excite the goal coefficients for the slotted array. The feeding network implementation is illustrated in Section 3 with the complete analysis of the proposed modified power splitter in the feeding network. The verification of the simulated results with the measured ones after the fabrication of the prototype array antenna is confirmed in Section 4. Finally, the conclusion is briefly discussed in Section 5.

2. ANTENNA ARRAY DESIGN

In Fig. 1, the perspective view of the proposed multilayered antenna array structure, which consists of micro machined layers

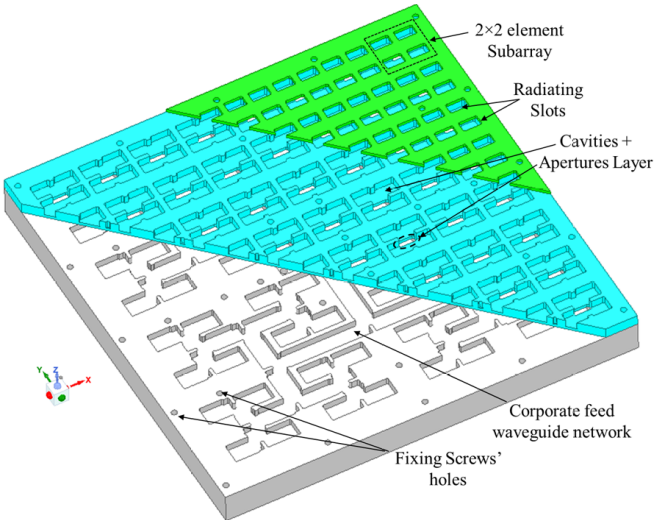

FIGURE 1. The configuration of the Ku-band 16×16 slot array antenna.

aligned together using screws. The layers are arranged from top to bottom as follows: radiating slot layer, cavity backed layer, aperture layer, and feeding network layer. The feeding network in this antenna is a full-corporate feeding network composed of many H-plane even/uneven power dividing T-junctions connected together. At the end of the rectangular waveguides in the feeding network there exist coupling apertures with offset locations to assure maximum excitation to the upper cavity layer. The cavity layer is excited from the coupling apertures in the previous layer and centered in the cavity which splits the power equally through existing walls in the x and y directions. Each cavity in the cavity layer resonates, and the radiation comes out through the equally spaced radiating slots in the upper top plane.

The proposed multilayered slotted array antenna design can be divided into three main parts: the subarray building cell, the excitation coefficients required to be excited from the radiating slots (according to the used array synthesizing technique), and the feeding network utilizing modified power splitters to achieve the needed coefficients. In each section, the methodology and design equations used in the design are declared and verified with the simulation results to guarantee the required goal of each phase in the design.

2.1. 2×2 Even Power Distribution Subarray Cell

The building unit of the array is shown in Fig. 2. The 2×2 even power distribution subarray unit cell (EPSC) is excited from the ends of the waveguides in the feeding network where coupling apertures are located with offset position to maximize the excitation to the above cavity. The cavity dimensions are optimized to have their resonance with a wide bandwidth in the Ku-band. The design frequency of the antenna is 15 GHz, and the radiating slots are spaced in both x and y directions with fixed spacing S_0 from center to center $(0.75\lambda_0)$ which is less than one wavelength to avoid grating lobes occurrence. The subarray is simulated using EM simulation software (Ansys HFSS) to verify the performance of the model.

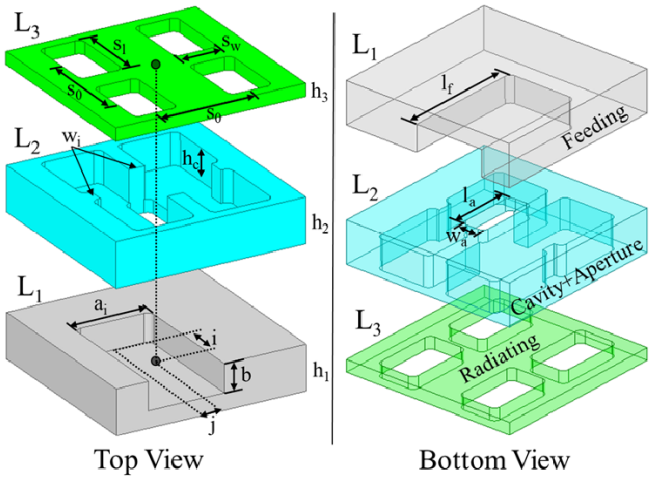

FIGURE 2. 3D layout for the Ku-band 2×2 subarray.

As shown in Fig. 3, the magnetic field is coupled from the feeding layer to the cavity of the subarray where the magnetic field distribution in the cavity of the subarray is symmetrical along the y direction. The excitation of the magnetic field comes from the magnetic field of the TE_{10} mode in the feed waveguide exciting the coupling aperture at the end mainly with the x component. The radiating slots' length and width (S_l, S_w) control the center frequency and bandwidth of the cavity, and the height of the cavity (h_c) has a role in controlling them.

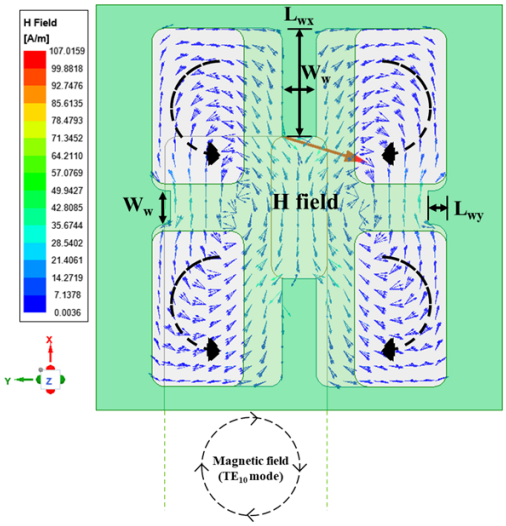

FIGURE 3. The magnetic field distribution in the cavity of the 2×2 EPSC.

The side walls located in the x and y directions are responsible for suppressing unwanted higher modes, and varying the length of these walls (L_{wx}, L_{wy}) has an impact in enhancing the matching impedance for the resonance of the cavity. The subarray radiation is shown in Fig. 4, where the voltage standing wave ratio (VSWR) is less than 2, and the bandwidth (BW) percentage is about 10% with respect to the center frequency. The bandwidth is adjusted with the aid of:

i. Adjusting both dimensions of the radiating slots.

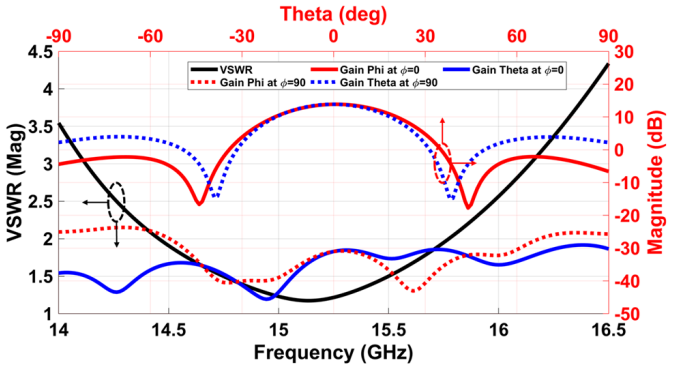

FIGURE 4. The operating bandwidth and Co- and Xp-radiation patterns for the 2×2 subarray.

ii. Adjusting both (j, i) parameters which indicate the shift of the feeding waveguide center and end to the center of the coupling slot, respectively.

iii. Adjusting the lengths of the cavity conducting walls (L_{wx}, L_{wy}).

All the dimensions of the proposed EPSC are demonstrated in Table 1. The sidelobe levels in E- and H-planes are -11 and -16 dB, respectively, as the uniform array behavior, while in the next sections the non-even power distribution coefficients technique is illustrated in order to obtain a nonuniform array behavior. The cross-polarization discrimination between Co- and Xp-components in each plane is better than -30 dB. The gain of this subarray is 13.9 dBi as shown in Fig. 4 in both E/H-planes. Also, the performance of the 3D-polar gain pattern of the subarray unit-cell (SU) is demonstrated in Fig. 5. This analysis has been done using commercial software (ANSYS HFSS).

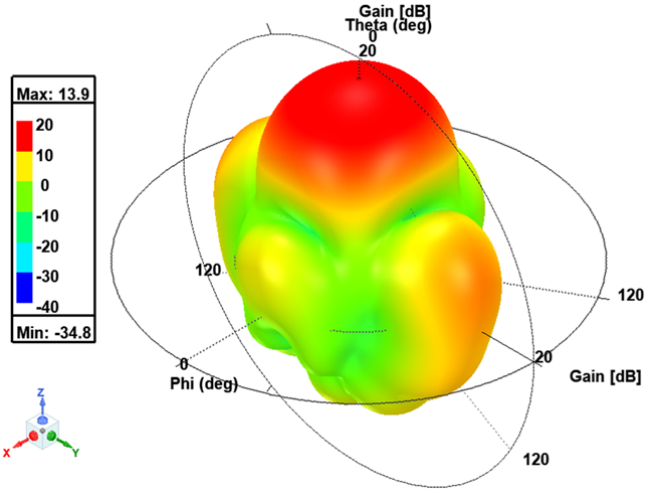

FIGURE 5. The 3D polar radiation gain pattern for the SU.

2.2. The Array Synthesis and Feeding Network

The target sidelobe level in the proposed design is 30 dB with Taylor synthesis [28] employed to adjust the power amplitudes along the radiation slots with uneven values. The performance of the whole network is expected to be lower than the target designed levels, due to the losses of leakage of EM waves from

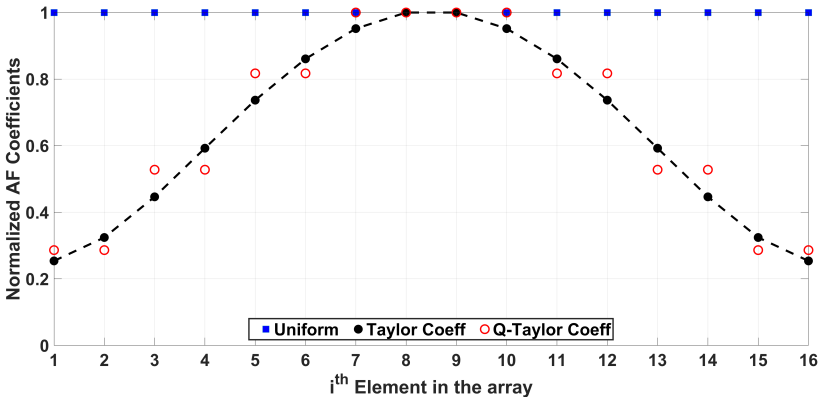

FIGURE 6. The array factor coefficients of the uniform, Taylor, and Quasi-Taylor array synthesis.

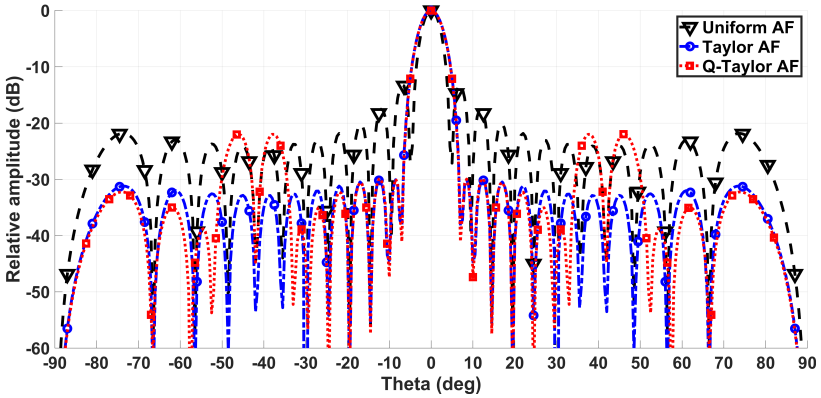

FIGURE 7. The comparison between array factors utilized with different synthesize techniques with 16×16 elements.

TABLE 1. The dimensions of EPSC.

Parameter	Value [mm]	Discribtion
a_i	12	Waveguide width of i order
b	4.4	Waveguide height
h_1	7	Feeding layer thickness
h_2	7	Aperture + Cavity thickness
h_3	2	Radiating slot layer thickness
h_c	5	Cavity thickness
l_a	10.5	Length of aperture
L_{wx}	8	Length of the cavity wall$_X$
L_{wy}	1.4	Length of the cavity wall$_Y$
S_l	11.5	Radiating slot length
S_w	6.8	Radiating slot width
S_0	15	Radiating slot spacing center-to-center
w_a	4.1	Width of aperture
W_w	2.5	Width of the cavity walls$_{X,Y}$

the layers (relates to the imperfect electrical contact and surface roughness of the multilayer faces), and the tolerance of fabrication precision (CNC milling and DLS accuracy).

The values of the distributed power coefficients for the 16-element linear array according to Taylor calculations are shown in Fig. 6 with radiating slots spacing $0.75\lambda_0$ from center-to-center. In the case of the proposed array antenna excited with 8×8 coupling apertures, each aperture excites 2×2 EPSC, and the power coefficients at each aperture are split into four even values at the radiating slots corresponding to Quasi-Taylor synthesizes (Q-Taylor) as shown in Fig. 6, in addition to comparing the coefficients of even, Taylor, and Q-Taylor. Also, the ideal normalized array factors of such E/H-plane of the 16×16 element array antenna with the prerequisite design specifications are calculated using both Taylor and Q-Taylor synthesized and compared with the even amplitude distribution as shown in Fig. 7.

The red coloured values within the parentheses represent the required power ratios for the corresponding 8×8 aperture slots. The synthesized array in this case has applied Taylor criteria till the output of the aperture slots with spacing $1.5\lambda_0$ as shown in Fig. 8. Then, the coefficients of the array are modified through the cavity layer, where the coefficients of the array factor are split into four equal magnitudes till the radiation slots with values shown in Fig. 6 become Q-Taylor in the end of the array synthesis.

For the sake of achieving the calculated coefficients at each aperture slot, an optimized feeding network should be designed with the minimum number of uneven power splitters within each T-junction. The 1-to-64 way corporate feed network is constructed using H-plane T-junctions of even and uneven power splitters (UPSs) to excite the apertures with the corresponding calculated power amplitudes as shown in Fig. 9. The input feeding of the array is fed with SMA, then the input sig-

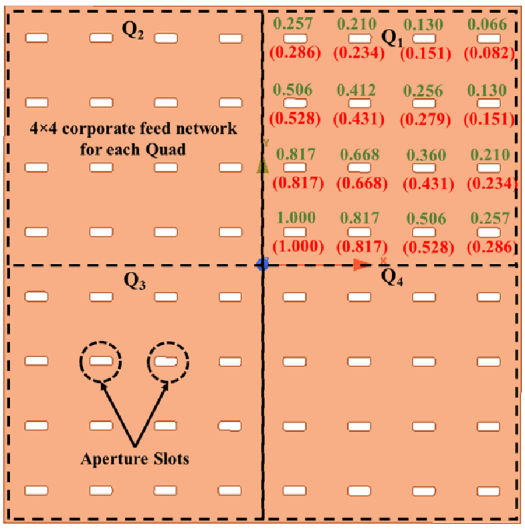

FIGURE 8. The uneven power distribution ratios.

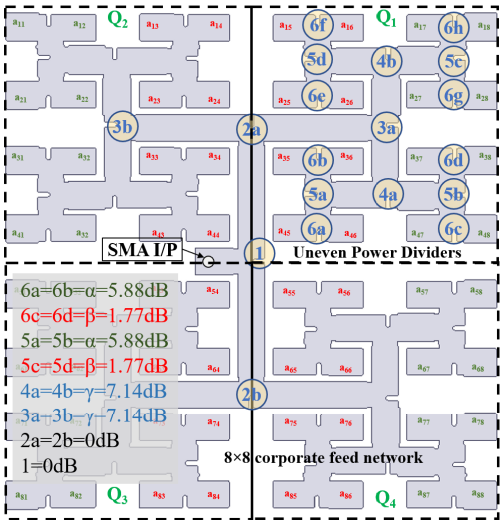

FIGURE 9. The corporate-feed waveguide network of uneven power dividers.

nal met three even power splitters (EPSs) (1, 2a, and 3a) after multiple UPSs have existed to meet the required excitations. Adjusting the output of each UPS port to match the designed values will be demonstrated in detail in the next section.

Based on the advantage of using Q-Taylor criteria in the array synthesis, only three optimized UPSs are necessary to build the designed planar power distribution coefficients with power splitting ratios: alpha $=$ 5.88 dB, beta $=$ 1.77 dB, and gamma $=$ 7.14 dB to make the network design simple with minimum number of UPSs used. These values are obtained from one of the optimized scenarios to use a minimum number of UPSs, and they could be with other values but depending on the power splitting ratio limit values according to the applied splitter.

As the feeding network is mirrored in both horizontal and vertical directions $(x, y$-directions), only one quarter of the feeding network (Q1: 4×4-network) is illustrated in both Fig. 8 and Fig. 9, displaying the simulated target field amplitudes with the green color above the designed amplitudes inside the parentheses with the red colour, in which there is big matching between the optimized feeding network values and designed values.

3. THE FEEDING NETWORK IMPLEMENTATION

The main objective of this section is to explain how to implement the early designed feeding network. The implementation challenge is to achieve the calculated power ratios, and at the same time, all the divided powers that have been realized using rectangular waveguides are in phase.

As discussed in the previous section, constructing the feeding network according to Q-Taylor tapering criteria decreases the sidelobe levels of the proposed Ku-band array. The challenge in this section is to design a passive uneven-power splitter to obtain the optimized power ratios in the feeding network in order to get a low sidelobe level array to the required design levels while keeping the phase at the output ports of each splitter balanced. In Fig. 10, the principle of splitting power is represented in the wedge with width (w_2) and length (h_2) in which the splitting ratio is obtained from the equivalent offset distance $(d_{offseti})$ for the wedge of the specific splitter 'i' in the network. In addition to splitting the power, it is necessary to keep the input port of the splitter matched along the operating bandwidth, which has been achieved with the aid of the two wedges at the end of port 1 as in Fig. 10 to be fixed for all the splitters in the feeding network of length (h_1) and width (w_1).

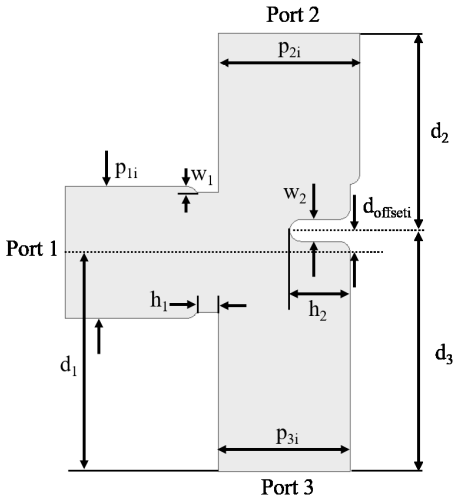

FIGURE 10. The construction of an uneven power splitter used in the proposed Ku-band array.

The achieved balanced phase with splitting the power in different ratios simultaneously is carried out by varying the width of port 2 in each splitter to compensate the difference in phase shifts of the magnetic field at output ports 2 and 3. Only the width of one port is changed to keep the balance of phases at the outputs while the second output port width is kept the same as the width of input port 1. The phase difference that occurs in the two output ports, as previously stated, primarily results

from the unequal propagation distances of the waves from the input port. It is possible to adjust the wave velocities within the T-junction to attain phase equilibrium in this scenario. A set of mathematical expressions has been formulated to determine the estimated output-port width (e.g., P_{2i}), which also has been considered a crucial role in determining guide-wave velocities and ultimately influencing output phases. In order to calculate the required width for a specific offset distance, it can be obtained from the following equations:

$$\lambda_c = \frac{2}{\sqrt{\left(\frac{m}{P}\right)^2 + \left(\frac{n}{B}\right)^2}} \tag{1}$$

$$k = \frac{2\pi}{\lambda}\sqrt{1 - \left(\frac{\lambda}{\lambda_c}\right)^2} \tag{2}$$

$$k_2 \times d_2 = k_3 \times d_3 \tag{3}$$

$$P_{2i} = \frac{\lambda}{2\sqrt{1 - \left(\frac{d_1 + d_{offseti}}{d_1 - d_{offseti}}\right)^2 \left(1 + \frac{\lambda}{2a_{3i}}\right)\left(1 - \frac{\lambda}{2a_{3i}}\right)}} \tag{4}$$

where λ_c is the cut-off wavelength in the waveguide, k the wavenumber of TE_{10} mode in the waveguide, d the distance of propagation in each port, and P_i the width of the ith port in any UPS in the proposed designed network.

The wave propagated in UPS should have different phases at the output ports (2, 3) of the conventional T-junction uneven power splitter (CUPS), so this can be compensated by adjusting only one port width of the output ports to keep the phase velocity of the split wave equal at the outputs. In order to calculate the phase velocity, substitute (1) in (2) and then apply (3) to maintain constant phase velocity. The adjustable width at the output of any modified uneven power splitter (MUPS) in the proposed feeding network could be calculated using (4) where ($d_3 = d_1 + d_{offset}$, $d_{23} = d_1 - d_{offset}$).

The phase difference between the output ports in the CUPS is shown in Fig. 11(a) where the TE_{10} wave splits into uneven ratios, and it is noticed that there is a difference in the displacement at ports 2 and 3 ends. On the other side in Fig. 11(b), the TE_{10} wave splits unevenly thanks to the adjustable waveguide width at port 2 while keeping the width of port 3 constant, the same as port 1, which helps in balancing the phase at both ends of the both ports.

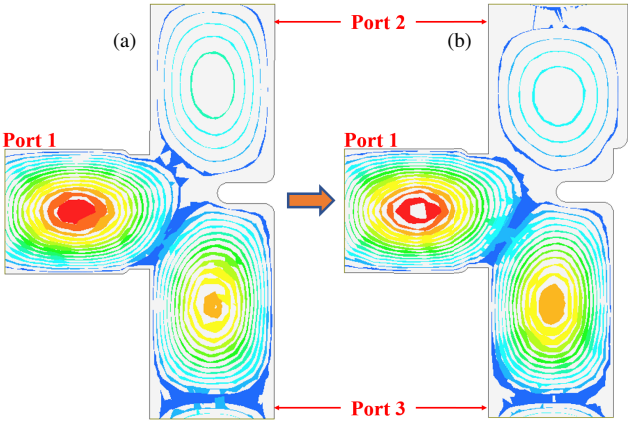

FIGURE 11. The electric-field distribution in both (a) conventional UPS, and (b) modified UPS.

The three basic MUPSs in the proposed designed parallel feeding network, alpha, beta, and gamma splitters, have been studied as shown in Fig. 12, where the matching from input port 1 (S_{11}) of each MUPS is below -20 dB, and the splitting ratios for both ports (2, 3) are observed in S_{21} with circle mark and S_{31} with square, respectively.

Also, the magnitude of power ratios between the output ports (2, 3) of the three main UPSs in CUPS represented by the dashed curves with edged colored marks compared to the power ratios in MUPS represented by the solid line curves with full-colored marks are shown in Fig. 13(a) with the required splitting values at the center frequency 15 GHz. It is obvious that the magnitudes of these ratios are almost around the required values within the rest bandwidth except that gamma UPS splitting ratio in the upper band deviates a little more than the other two UPSs (beta and alpha) as it is the largest splitting ratio in the feeding network.

The phase difference between the output ports is shown in Fig. 13(b) where there is a large phase difference of the three CUPSs with a maximum phase deviation of 47 degrees within the entire band represented by dashed lines with edged colored marks, while the maximum phase difference in the case of using the three MUPSs is 19 degrees represented with solid lines with full-colored marks which is much less than the phase difference of CUPS, and it can be considered less than 15 degrees within the operating frequency band of the proposed array. The proposed MUPS has almost zero phase difference at the center frequency of 15 GHz with good matching below -20 dB. The corresponding lengths for both offset distances and output port widths are declared in Table 2 to achieve the target splitting ratios.

TABLE 2. The dimensions of the corresponding offset distance for wedges and output port widths.

Parameter	Value [mm]		
-	gamma	alpha	beta
d_{offset}	1.4	1.16	0.38
P_2	13.1	12.75	12.21

4. EXPERIMENTAL RESULTS

4.1. Fabrication and Matching Validation

The Ku-band array antenna is fabricated with size ($12\lambda_0 \times 12\lambda_0 \times 0.8\lambda_0$) using DLS and CNC milling technologies. The radiation performance is also measured inside an anechoic chamber using a compact range measuring system as shown in Fig. 14(a). The multilayer construction of the proposed antenna is shown in Fig. 14(b), and the side and bottom views of the attached construction are shown in Fig. 14(c) and Fig. 14(d), respectively. The layers of the proposed array are attached together with the aid of fixing screws allocated through the network to attach all the layers tightly to avoid EM leakage. The EM leakage in the feeding network causes transmission loss to

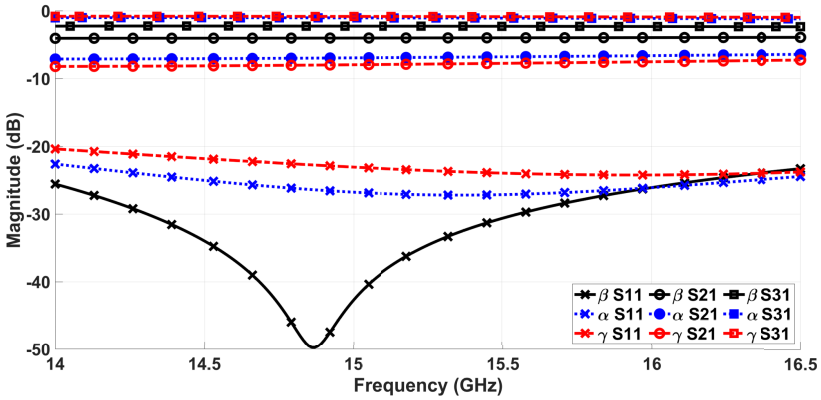

FIGURE 12. The S-parameters of the three main MUPS.

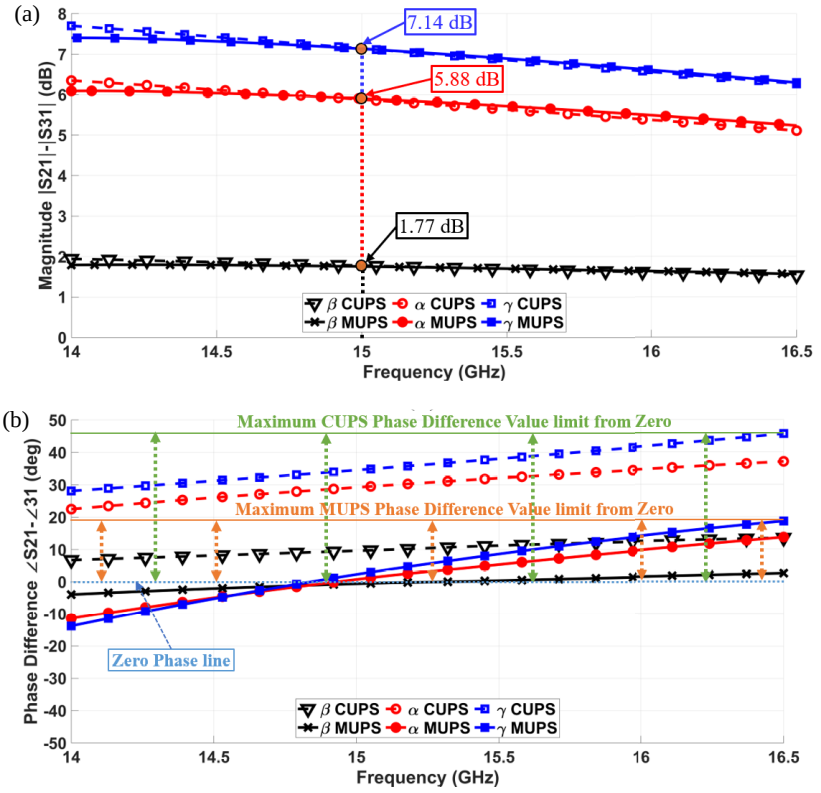

FIGURE 13. (a) The power ratios, and (b) the phase difference between the output ports, in each CUPS and MUPS.

the power at the radiating slots since the power distribution at the radiating slots is uneven with altered phases according to the parallel feeding network.

The VSWR for the proposed array antenna is shown in Fig. 15 which guarantees the matching at the input of the feeding waveguide network within 14% bandwidth. The radiation pattern of the proposed array is calculated using the numerical analysis techniques and simulated as shown in Fig. 16 at the center frequency of 15 GHz.

4.2. Experimental Radiation Pattern Analysis

As noticed, the beamwidth in the case of uneven power distribution AF is wider than that of the even case, and also there are two large minor lobes values between angles ± 30–45 degrees due to employing 2×2 EPSCs in the feeding stages underneath the radiating slots to perform Q-Taylor technique with 8×8 coefficients at the aperture layer, since each coupling aperture output is split into four even power portions for each radiating slot, instead of employing waveguides with uneven power of 16×16 coefficients in Taylor technique for the whole array.

The simulated and measured radiation pattern performances of the proposed Ku-band array antenna in both E- and H-planes are plotted as shown in Fig. 17 and Fig. 18, respectively. The first sidelobe level (FSLL) of -30 dB in the design considerations is almost achieved to be -25 dB in the E-plane and -28 dB in the H-plane at 15 GHz. The half-power beamwidth (HPBW) in both E- and H-planes at 15 GHz is 5/4.9 degrees,

TABLE 3. Previous work compared to the proposed Ku band array antenna.

Ref	Struct. Material	IB (GHz)		Freq. Band		Elem. No.	No. Lay.	Gain (dB)	RE (%)	SLL E/H (dB)	No UnEq. PD	Fab. Cost	Dim. (λ_0)
		mag	(%)	Cent.	Band								
[29]	SIW+IMGW	6	16	37.5	Ka	8×8	4	24	41.69	18	6	Low	8.125×8.125×0.17
[30]	SIW+RGW	12	35.3	34	Ka	4×4	4	16	13.8	12.1/15.6	2	High	5.66×5.66×0.3
[31]	Metallic-IMGW	9	17.6	60	V	16×16	4	29	50	23	4	Med	13.2×13.2×1.02
[32]	3DPrinted-RGW	7.3	18%	39.5	Ka	16×16	4	32	60	18(ETSI)	0	High	16.67 ×16.67×2.3
[33]	3DPrinted-HM-GGW	2.17	7	30	Ka	8×8	2	26.6	84	22	3	High	8.8×8×1.2
[34]	Metallic-RGW	5	5.7	85	W	16×18	3	29.4	60	19.7/30	7	Med	NA
[35]	Metallic-R/GGW	1.2	4.3	28	Ka	16×16	6	28	50	18.5(y)/19.5(x)	3	High	NA
[36]	Metallic-RGW	3.3	11	30	Ka	8×8	2	26	82	20	3	High	10×10×0.97
[40]	Metallic-PCB	15	19	78.5	E	32 CST	6	40	74	25.5/25.5	-	High	30.3×29.5×3
[18]	Metallic-Diff Bonding	5	8.1	60	E	16×16	5	33	70	25.5/26.1	-	High	15.3×15.5×1.35
[19]	Metallic-Diff Bonding	15	19	78.5	E	16×16	6	32.9	86.6	27.1	-	High	15.7×16×0.83
[37]	Metallic	2	14	15	Ku	16×16	4	30.5	70	26.5/30.4	3	Med	12×12×0.72
[38]	Full Metallic	4	13.6	29	Ka	160planar slots	3	29	70	18	3	Med	11.1×8.5 ×1.07
[39]	Full Metallic	0.35	4	8.9	X	76planar slots	3	23.2	30	28.8	3	Med	7.27×7.27×NA
Paper	Full Metallic	2	14	15	Ku	16×16	3	32.12	90	27/30	3	Med	12×12×0.8

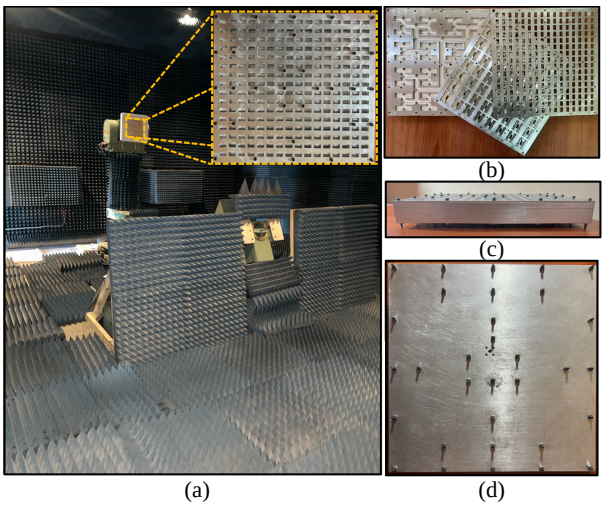

FIGURE 14. (a) The fabricated antenna measured in the in the anechoic chamber, (b) multilayer construction of fabricated antenna, (c) the side view and (d) the bottom view of the fabricated machined array antenna.

respectively. The cross-polarization discrimination (XPD) is obtained to be more than 40 dB at the design frequency.

To make sure of the performance stability, the proposed array antenna radiation pattern was reinvestigated at 14.5 GHz and 16 GHz, as will be illustrated in Fig. 19 and Fig. 20, respectively. At 14.5 GHz, the FSLLs for both E- and H-planes as in Fig. 19(a) and Fig. 19(b) are -24.5 and -27 dB, respectively. The HPBWs are obtained to be 5.3 and 5.2 degrees in E- and H-planes, respectively.

At 16 GHz, the FSLLs for E-/H-planes as in Fig. 20(a) and Fig. 20(b) to be -27 and -30 dB and HPBW are 4.8/4.7 degrees, respectively. The overall pattern performance using MUPs to build up the feeding network to apply Q-Taylor synthesis for the fabricated array is accepted.

4.3. Directivity, Efficiency Analysis and Performance Comparisons

The gain, directivity, and efficiency parameters for the proposed Ku-band are shown in Fig. 21 since the array gain has been measured in a compact range system inside an anechoic chamber using standard gain horn antennas for both Tx and Rx. There is a good match between the simulated gain and the measured one as marked in a solid black curve with circle marks and a dotted black curve with square marks, respectively. The measured gain at the center frequency 15 GHz is 31.5 dB, and the max peak gain within the operating band is 32.12 dB. Also, the efficiency of the array is obtained from the directivity and measured gain. The efficiency of the fabricated array as shown in Fig. 21 is high above 90% along the bandwidth. The rest of the losses in the efficiency may be from any wave leakage between the layers of the multi-layer array, the precision of the milling process, and the uneven power distribution in Q-Taylor array different from the even power distribution which impacts the gain, beamwidth, and efficiency.

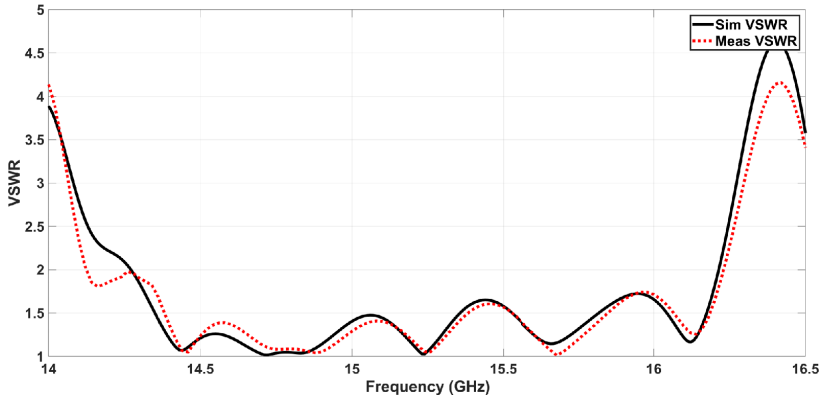

FIGURE 15. The reflection performance of the Ku-band array antenna.

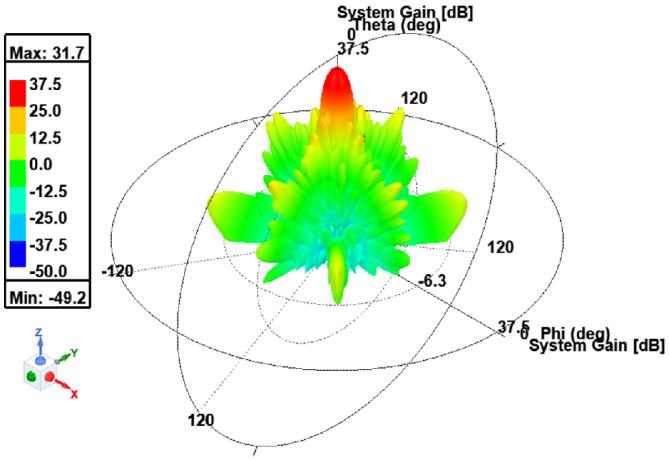

FIGURE 16. The 3D polar plot for the system gain of the Ku-band array antenna at 15 GHz.

The previous works in such antennas are compared in Table 3, and all the previous works in the table are array antennas with low sidelobe while the proposed work has the advantage of high gain and radiation efficiency compared to the arrays in the same band or even with scaling to upper bands. In radar applications, every increased value in both gain and efficiency helps in target detections at more ranges with the narrow beam for radar resolution for target discrimination. Also, it is not preferable to use array antennas with printed circuit board (PCB) laminates in the structure to avoid dielectric loss and keep handling the high power as in [29–31]. The gap waveguide technology is applied in arrays and fabricated using 3D printing technology as in [32, 33] where the durability of such structures in radar applications is not better than the full metallic rigid antennas besides the high cost for fabrication especially for mass production. In [34], a full metallic array antenna has been proposed with a hybrid feeding planar network which is not recommended for wide-range radar antennas to keep the advantage of switching between different frequencies over the band to overcome any jamming attacks besides its poor radiation efficiency over the entire band. In [35], a dual-polarized array with low sidelobe level is introduced with multi-layers using four different power splitters to perform the required excitation at radiating slots which make the structure bulkier and the sidelobe levels not enough to serve in radar applications efficiently. In [36], an 8×8 Ka-band antenna array with a full metallic body and the feeding network utilized Taylor amplitude tapering to feed the 64 slots directly from the waveguide ends. The authors avoided using cavities before the radiating slots in order to avoid the undesired lobes at angles 35–45 degrees since there is much spacing in the 8×8 array to feed directly without cavities, and the 20 dB SLL is also not enough for radar application although it has good 82% radiation efficiency. Another way to perform low sidelobe in arrays is by applying 45° linear polarizer silver plated with a polycarbonate substrate on a uniform array, to decrease the radiation envelope and shift the linear polarization to the required plane of low SLL, which is high-cost fabrication and also affects the radiation efficiency as mentioned before because of using laminates on the top of the array. Refs. [18, 19] used a 45° linearly polarized planar feed by using an extra layer on the top of the radiating slots that make defecting radiation patterns and radiating efficiencies, and these array antennas are fabricated using diffusion bonding technology which is much more expensive than conventional CNC machining. In [37], the antenna design has the same synthesis as the proposed paper, but with difference in the optimized modified power splitters to perform more efficiently to avoid any multi-reflections from the intersection of different power splitters in the feeding networks which cause degradation in radiation efficiency and gain of the antenna. In radar applications, it is preferable to use more efficient arrays with the best performance over the entire band which is the main goal of the proposed work of introducing a simple detailed design of high-gain array antenna with low sidelobe and stable high gain, and radiation efficiency over the entire band operating in the Ku-band where many radar devices have a big interest in this band. Finally, in [38, 39] the arrays introduced in both are designed using hybrid feeding between series and parallel networks which limits the operating band to be wide as long line effect in the series part, and the radiation efficiencies are also not better than the proposed work in this manuscript. In [40], 32-slot Continuous Transverse Stub (CTS) array with low SLL using a 45° linear polarizer operating at 78.5 GHz frequency with multi-layered complex feeding networks must be implemented with minimum fabrication tolerance in addition to the polarizer layers to the 32-slot CTS array simulation which needed more computational power that did not exist and only depend on the simulations of the smaller array performance with the polarizer.

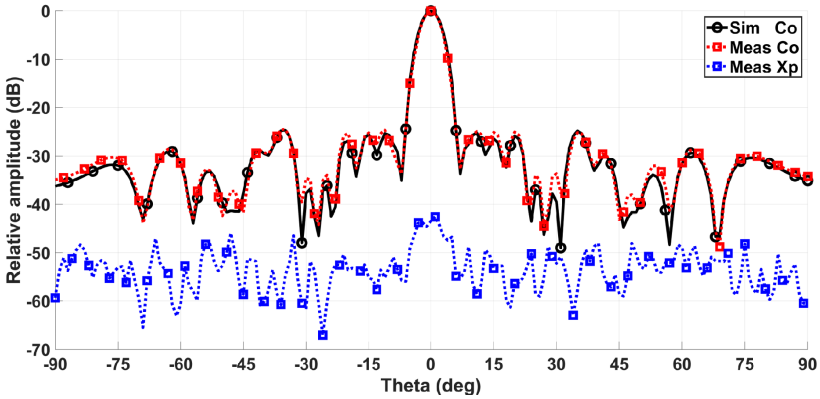

FIGURE 17. The far-field radiation pattern for E-plane at 15 GHz.

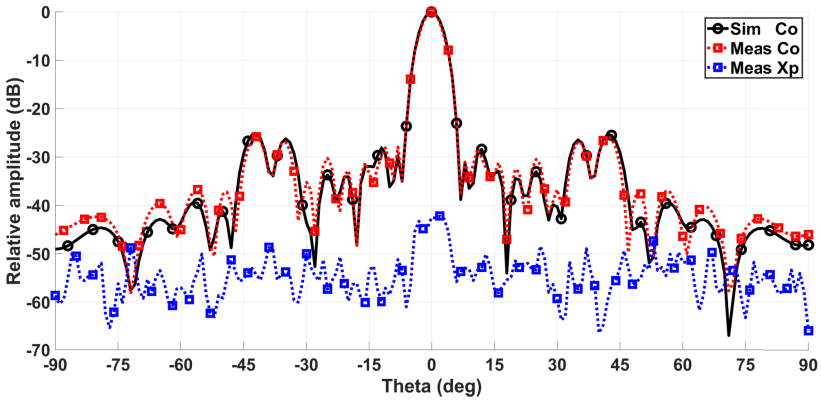

FIGURE 18. The far-field radiation pattern for H-plane at 15 GHz.

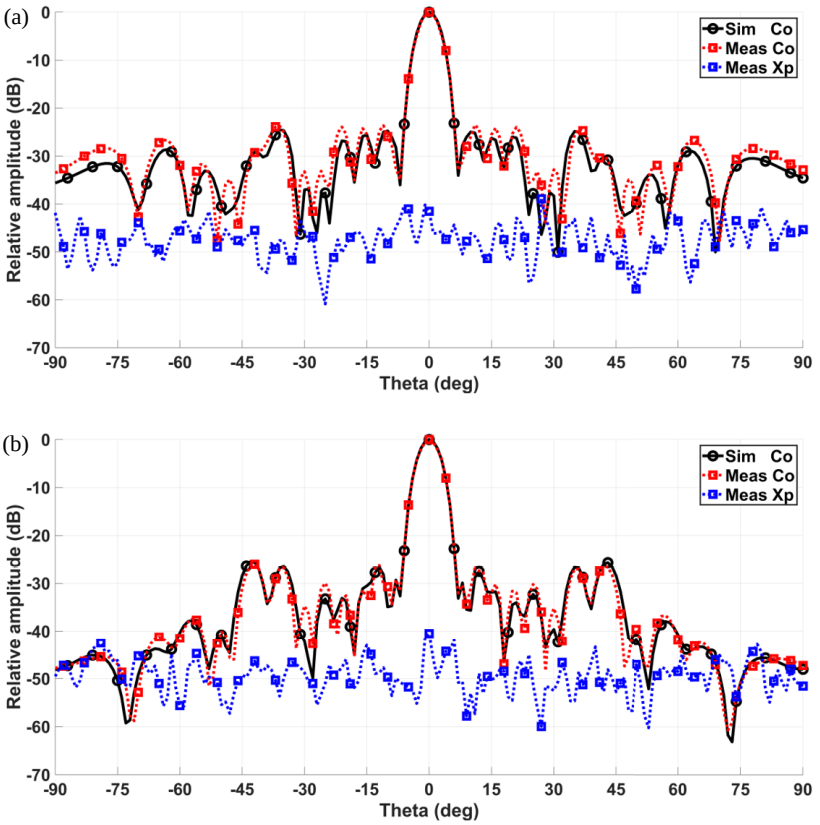

FIGURE 19. The far-field radiation pattern for both (a) E-plane and (b) H-plane at 14.5 GHz.

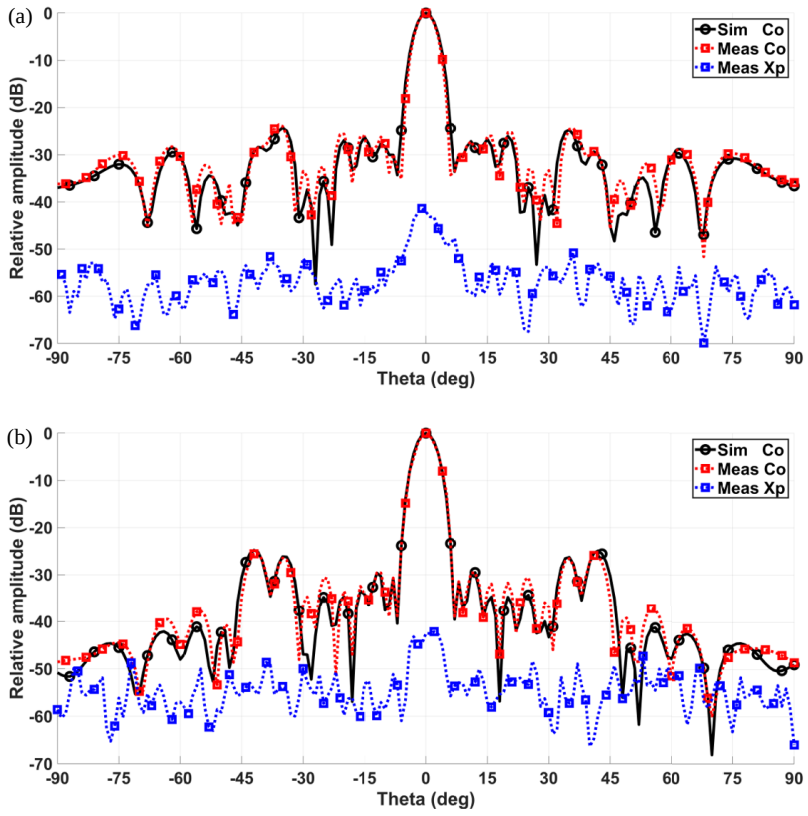

FIGURE 20. The far-field radiation pattern for both (a) E-plane and (b) H-plane at 16 GHz.

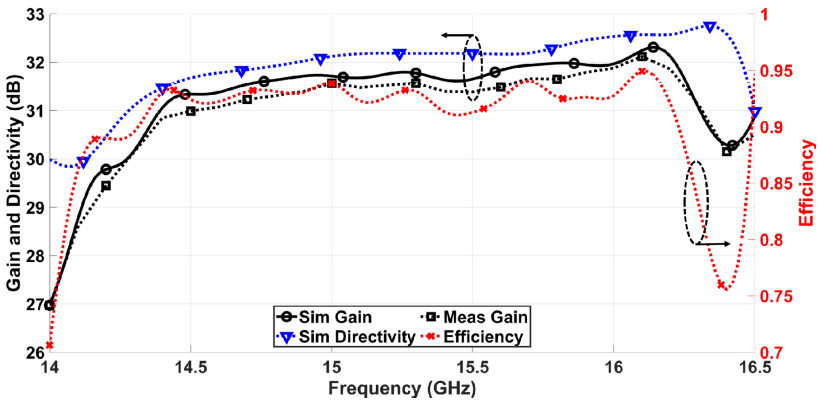

FIGURE 21. The directivity of the full Ku array with the simulated and measured gain antenna and the radiation efficiency.

5. CONCLUSION

A high efficient 16×16 Ku-band slotted array antenna has been designed using a parallel multi-layer feeding network to achieve Q-Taylor power distribution of uneven coefficients to an 8×8 coupling aperture array using MUPS. The output of each coupling aperture feeds a 2×2 EPSC reaching the radiating slots. Also, the proposed array antenna has been efficiently fabricated using DLS and CNC milling processes and measured to verify the efficiency of the MUPS used in the feeding network where, the bandwidth is almost 14% with low sidelobe level of -28 dB at the centre frequency 15 GHz and HPBW 5/4.8 degrees for E-/H-planes, respectively. The measured gain is 31.5 dB with XPD more than 40 dB and efficiency above 90%.

REFERENCES

[1] Lemberg, K. V., O. A. Nazarov, V. S. Panko, and Y. P. Salomatov, "High gain substrate integrated waveguide slot antenna array," in *2015 International Siberian Conference on Control and Communications (SIBCON)*, 1–3, Omsk, Russia, 2015.

[2] Kim, D.-Y., W. Chung, C. Park, S. Lee, and S. Nam, "Design of a 45°-inclined SIW resonant series slot array antenna for Ka-band," *IEEE Antennas and Wireless Propagation Letters*, Vol. 10, 318–321, 2011.

[3] Patanvariya, D. G. and A. Chatterjee, "High gain and low cross-polarized printed array of Baravelle's spiral antennas for Ku-band application," *AEU — International Journal of Electronics and Communications*, Vol. 132, 153634, 2021.

[4] James, J. R., P. S. Hall, and C. Wood, *Microstrip Antenna: Theory and Design*, Peter Peregrinus, London, 1986.

[5] Cheng, Y. J., Y. X. Guo, and Z. G. Liu, "W-band large-scale high-gain planar integrated antenna array," *IEEE Transactions on Antennas and Propagation*, Vol. 62, No. 6, 3370–3373, 2014.

[6] Nissanov, U. and G. Singh, "Beamforming D-band phased array microstrip antennas," *Sensors International*, Vol. 3, 100196, 2022.

[7] Emara, H. M., S. K. E. Dyasti, H. H. Ghouz, M. F. A. Sree, and S. Y. A. Fatah, "Compact high gain microstrip array antenna using DGS structure for 5G applications," *Progress In Electromagnetics Research C*, Vol. 130, 213–225, 2023.

[8] Wang, S., D. Zhang, Z. Ding, H. Chen, and S. Yang, "Broadband proximity coupled millimeter-wave microstrip array antenna for automotive radar applications," *Progress In Electromagnetics Research Letters*, Vol. 107, 93–101, 2022.

[9] Shirkolaei, M. M., "High efficiency X-band series-fed microstrip array antenna," *Progress In Electromagnetics Research C*, Vol. 105, 35–45, 2020.

[10] Chen, Z., S.-G. Zhou, and T.-H. Chio, "A class of all metal cavity-backed slot array with direct metal laser sintering," *IEEE Access*, Vol. 6, 69 650–69 659, 2018.

[11] Zhang, M., K. Toyosaki, J. Hirokawa, M. Ando, T. Taniguchi, and M. Noda, "A 60-GHz band compact-range gigabit wireless access system using large array antennas," *IEEE Transactions on Antennas and Propagation*, Vol. 63, No. 8, 3432–3440, 2015.

[12] Arakawa, H., H. Irie, T. Tomura, and J. Hirokawa, "Suppression of E-plane sidelobes using a double slit layer in a corporate-feed waveguide slot array antenna consisting of 2×2-element radiating units," *IEEE Transactions on Antennas and Propagation*, Vol. 67, No. 6, 3743–3751, 2019.

[13] Ghorbani, S., S. A. Razavi, M. H. Ostovarzadeh, and A. Farahbakhsh, "Development of a center fed slot array antenna with very low side lobes using ridge gap waveguide (RGW) technology," *AEU — International Journal of Electronics and Communications*, Vol. 125, 153385, 2020.

[14] Alessandri, F., M. Mongiardo, and R. Sorrentino, "Computer-aided design of beam forming networks for modern satellite antennas," *IEEE Transactions on Microwave Theory and Techniques*, Vol. 40, No. 6, 1117–1127, 1992.

[15] Poulton, G. T., T. S. Bird, S. G. Hay, and Y. K. Choi, "Rigorous design of an antenna for AUSSAT-B," in *International Symposium on Antennas and Propagation Society, Merging Technologies for the 90's*, 1900–1903, Dallas, TX, USA, 1990.

[16] Moradian, M., "Employing the dumbbell-shaped longitudinal slot antennas in the planar slotted antenna arrays," *International Journal of Microwave and Wireless Technologies*, Vol. 14, No. 7, 914–925, 2022.

[17] Miura, Y., J. Hirokawa, M. Ando, Y. Shibuya, and G. Yoshida, "Double-layer full-corporate-feed hollow-waveguide slot array antenna in the 60-GHz band," *IEEE Transactions on Antennas and Propagation*, Vol. 59, No. 8, 2844–2851, 2011.

[18] Tomura, T., Y. Miura, M. Zhang, J. Hirokawa, and M. Ando, "A 45° linearly polarized hollow-waveguide corporate-feed slot array antenna in the 60-GHz band," *IEEE Transactions on Antennas and Propagation*, Vol. 60, No. 8, 3640–3646, 2012.

[19] Tomura, T., J. Hirokawa, T. Hirano, and M. Ando, "A 45° linearly polarized hollow-waveguide 16×16-slot array antenna covering 71–86 GHz band," *IEEE Transactions on Antennas and Propagation*, Vol. 62, No. 10, 5061–5067, 2014.

[20] Kim, D., J. Hirokawa, M. Ando, J. Takeuchi, and A. Hirata, "64×64-element and 32×32-element slot array antennas using double-layer hollow-waveguide corporate-feed in the 120 GHz band," *IEEE Transactions on Antennas and Propagation*, Vol. 62, No. 3, 1507–1512, 2014.

[21] Garcia-Marin, E., J. L. Masa-Campos, and P. Sanchez-Olivares, "Diffusion bonding manufacturing of high gain W-band antennas for 5G applications," *IEEE Communications Magazine*, Vol. 56, No. 7, 21–27, 2018.

[22] Le Sage, G. P., "3D printed waveguide slot array antennas," *IEEE Access*, Vol. 4, 1258–1265, 2016.

[23] Tak, J., A. Kantemur, Y. Sharma, and H. Xin, "A 3-D-printed W-band slotted waveguide array antenna optimized using machine learning," *IEEE Antennas and Wireless Propagation Letters*, Vol. 17, No. 11, 2008–2012, 2018.

[24] Garcia-Marin, E., J.-L. Masa-Campos, P. Sanchez-Olivares, and B. Guilarte-Bellod, "3D-printed frequency-scanned slot array in grating waveguide," *AEU — International Journal of Electronics and Communications*, Vol. 138, 153866, 2021.

[25] Jung, K., H.-Y. Lee, G.-C. Kang, S.-H. Han, and B. Lee, "Cavity-backed planar slot array antenna with a single waveguide-fed sub-array," in *IEEE Antennas and Propagation Society Symposium*, Vol. 3, 3273–3276, Monterey, CA, USA, 2004.

[26] Lee, B., K. Jung, and S.-H. Yang, "High-efficiency planar slot-array antenna with a single waveguide-fed cavity-backed subarray," *Microwave and Optical Technology Letters*, Vol. 43, No. 3, 228–231, 2004.

[27] Oh, S.-S., J.-W. Lee, M.-S. Song, and Y.-S. Kim, "Two-layer slotted-waveguide antenna array with broad reflection/gain bandwidth at millimetre-wave frequencies," *IEE Proceedings — Microwaves, Antennas and Propagation*, Vol. 151, No. 5, 393–398, 2004.

[28] Hansen, R. C., *Phased Array Antennas*, 2nd ed., John Wiley & Sons, 2009.

[29] Jiang, X., F. Jia, Y. Cao, P. Huang, J. Yu, X. Wang, and Y. Shi, "Ka-band 8×8 low-sidelobe slot antenna array using a 1-to-64 high-efficiency network designed by new printed RGW technology," *IEEE Antennas and Wireless Propagation Letters*, Vol. 18, No. 6, 1248–1252, 2019.

[30] Li, T. and Z. N. Chen, "Wideband sidelobe-level reduced Ka-band metasurface antenna array fed by substrate-integrated gap waveguide using characteristic mode analysis," *IEEE Transactions on Antennas and Propagation*, Vol. 68, No. 3, 1356–1365, 2020.

[31] Liu, J., F. Yang, K. Fan, and C. Jin, "Unequal power divider based on inverted microstrip gap waveguide and its application for low sidelobe slot array antenna at 39 GHz," *IEEE Transactions on Antennas and Propagation*, Vol. 69, No. 12, 8415–8425, 2021.

[32] Vosoogh, A., P.-S. Kildal, and V. Vassilev, "Wideband and high-gain corporate-fed gap waveguide slot array antenna with ETSI Class II radiation pattern in V-band," *IEEE Transactions on Antennas and Propagation*, Vol. 65, No. 4, 1823–1831, 2017.

[33] Castellá-Montoro, A., M. Ferrando-Rocher, J. I. Herranz-Herruzo, and A. Valero-Nogueira, "Low-sidelobe flat panel array fed by a 3D-printed half-mode gap waveguide amplitude-tapering network," *IEEE Access*, Vol. 12, 2607–2614, 2024.

[34] Li, L., J. Chen, L. Kong, P. Zhang, Q. Lv, B. Zhang, B. Tian, and C. Jin, "W-band ridge gap waveguide slot array antenna with low sidelobe and high-gain characteristics," *Microwave and Optical Technology Letters*, Vol. 64, No. 3, 565–570, 2022.

[35] Ran, J., C. Jin, P. Zhang, W. Wang, and Y. Wu, "High-gain and low-loss dual-polarized antenna array with reduced sidelobe level based on gap waveguide at 28 GHz," *IEEE Antennas and Wireless Propagation Letters*, Vol. 21, No. 5, 1022–1026, 2022.

[36] Pla-Herliczka, D., J. I. Herranz-Herruzo, M. Ferrando-Rocher, and A. Valero-Nogueira, "Taylor-weighting ridge gap waveguide feed network for low-profile fully metallic array antennas,"

IEEE Antennas and Wireless Propagation Letters, Vol. 23, No. 9, 2703–2707, 2024.

[37] Huang, G.-L., S.-G. Zhou, T.-H. Chio, H.-T. Hui, and T.-S. Yeo, "A low profile and low sidelobe wideband slot antenna array feb by an amplitude-tapering waveguide feed-network," *IEEE Transactions on Antennas and Propagation*, Vol. 63, No. 1, 419–423, 2015.

[38] Shi, L., C. Bencivenni, R. Maaskant, J. Wettergren, J. Pragt, and M. Ivashina, "High-efficiency and wideband aperiodic array of uniformly excited slotted waveguide antennas designed through compressive sensing," *IEEE Transactions on Antennas and Propagation*, Vol. 67, No. 5, 2992–2999, 2019.

[39] Kumar, P., A. Kedar, and A. K. Singh, "Design and development of low-cost low sidelobe level slotted waveguide antenna array in X-band," *IEEE Transactions on Antennas and Propagation*, Vol. 63, No. 11, 4723–4731, 2015.

[40] You, Y., Y. Lu, Y. Wang, W.-W. Yang, Z.-C. Hao, Q. You, and J. Huang, "High-performance E-band continuous transverse stub array antenna with a 45° linear polarizer," *IEEE Antennas and Wireless Propagation Letters*, Vol. 18, No. 10, 2189–2193, 2019.